Received: 29 December 2022 | Revised: 7 April 2023 | Accepted: 10 April 2023

DOI: 10.1002/hyp.14880

RESEARCH ARTICLE

WILEY

Intra-event concentration–discharge relationships affected by hydrological connectivity in a karst catchment

Liu Hao[1] | Zhicai Zhang[1] | Xi Chen[2] | Qinbo Cheng[1] | Siliang Li[2] | Fujun Yue[2] | Tao Peng[3,4] | Lin Zhang[3,4]

[1]College of Hydrology and Water Resources, Hohai University, Nanjing, China

[2]Institute of Surface-Earth System Science, School of Earth System Science, Tianjin University, Tianjin, China

[3]Institute of Geochemistry, Chinese Academy of Sciences, Guiyang, China

[4]Puding Karst Ecosystem Research Station, Chinese Academy of Sciences, Guiyang, China

Correspondence
Zhicai Zhang, College of Hydrology and Water Resources, Hohai University, Nanjing 210098, China.
Email: zhangzhicai_0@hhu.edu.cn

Funding information
National Natural Science Foundation of China, Grant/Award Numbers: 42030506, 41971028, 42071039

Abstract

Concentration-discharge (C-Q) relationship in streamflow provides insights into hydrological transport at the catchment scale. Changes in hydrological connectivity during runoff events often dominate flood and solute export in the karst catchment. However, only few studies have explored intra-event C-Q relationships and how they are affected by hydrological connectivity in karst catchment. In this study, we explored the intra-event C-Q relationships in underground channel flows by integrating solute concentration, discharge and modelled flow age in a 1.25 km^2 karst catchment in southwest China. We apply piecewise functions to characterize the C-Q relationships on rising and falling limbs of hydrograph. Geogenic solutes exhibited dilution C-Q patterns during the runoff event, which could be fitted by two power-law models with different coefficients on rising and falling limbs. Affected by the strong hydrological connectivity between surface and subsurface, hillslope and depression, a steeper C-Q slope on the rising limb indicated an exhaustible, proximal source, that is, groundwater. In contrast, the C-Q patterns of the soil enriched solutes changed from enrichment to dilution during the runoff event. The enrichment pattern occurring at the early of rising limb was caused by strong hydrological connectivity between the surface and subsurface, which indicated a distal and plentiful sources of soil water. Whilst the strong hydrological connectivity between hillslope and depression caused a dilution pattern at the latter of rising limb. On the falling limb of hydrograph, a dilution pattern implied that the small fractures could be another source zone of soil-enriched solutes in addition to soil layer in the depression. The C-Q behaviours of soil-enriched solutes can be fitted by a combination of a parabola model and a power law model for rising and falling limbs, respectively. The current study highlights the variations in intra-event C-Q relationships of different solutes affected by hydrological connectivity in the karst catchment. Which is crucial for assession of hydrochemical processes and fertilization management in this area.

KEYWORDS
hydrological connectivity, intra-event C-Q relationship, karst catchment, water age

1 | INTRODUCTION

Karst catchment is characterized by unique heterogeneous and anisotropic hydrogeological conditions (Bakalowicz, 2005; Ford & Williams, 2013). Strong dissolution of carbonate rock makes a complex hydrogeological system, for example, different flow velocity and interconnected network paths in small fractures, large fractures and conduit (Hartmann et al., 2014). Variations in flow characteristics in these mediums with different hydraulic conductivities and storage capacities result in a marked spatiotemporal variability in hydrological processes. Under different wetness conditions, the sharp variations in hydrological connectivity between different landform units and between different mediums enhance the complexity of hydrological behaviours at the catchment scale (Hao et al., 2019). Specifically, the streamflow generation in intra-event is still an unanswered question for karst catchment, due to the variable flow paths and mixing processes controlled by hydrological connectivity (Benischke, 2021; Berglund et al., 2019; Ford et al., 2019). In karst environment, the transport and transformation of solutes are significantly related to hydrological processes, which makes it complicated to characterize the spatiotemporal variations in hydrochemistry in karst critical zone and down-stream (Husic et al., 2019, 2021; Yi et al., 2021; Yue et al., 2019, 2020; Zhang, Chen, Cheng, et al., 2020; Zhang, Chen, Zhang, & Soulsby, 2020). Although the process-based model by coupling hydrological and biogeochemical modelling can provide useful insights to this complexity, simulation of solute fate at the catchment scale usually requires detailed information of critical zone architecture (Husic et al., 2019; Zhang, Chen, Cheng, et al., 2020; Zhang, Chen, Zhang, & Soulsby, 2020). In addition, uncertainty often increases with the model complexity and parameters (Zhang & Shao, 2018).

The relationship between solute concentration and discharge (C-Q) establishes a linkage between solute dynamics at a given point in the stream to discharge, which provides a lumped insight to the hydrochemical processes at the catchment scale (Basu et al., 2011; Musolff et al., 2015; Stewart et al., 2022). C-Q relationships are usually linked to the solute availability (Westphal et al., 2020), hydroclimatic patterns (Dupas et al., 2016), flow paths (Hoagland et al., 2017), hydrological connectivity (Herndon et al., 2018), residence time (Tunaley et al., 2016), reaction kinetics (Ameli et al., 2017), and vegetation (Herndon et al., 2015). Which have been widely used to explore hydrological and reaction processes at the catchment scale (Knapp et al., 2020; Li et al., 2021; Musolff et al., 2017; Rose & Karwan, 2021). Many studies have approved that the C-Q relationships of streamflow can be used to assess solute behaviours under different hydrometeorological conditions in unique karstic environment (Xia et al., 2021; Yue et al., 2019; Zhong et al., 2018). Which have been extensively used to understand hydrological functions in karst catchment, and its responses to climate and land use change (Buckerfield et al., 2019; Zhang et al., 2021).

C-Q relationships are usually characterized at different temporal scale (Rose et al., 2018). The long-term and seasonal C-Q relationship can provide general patterns of hydrologic transport and associated controls (Minaudo et al., 2019; Westphal et al., 2020; Zarnetske et al., 2018). However, it cannot give enough information to reveal C-Q behaviours at the runoff event scale, the critical moment for flooding and export (Le Mesnil et al., 2022; Rue et al., 2017). With high frequency online observation and automatic sampling technique more available, more and more attentions focus on C-Q relationships at the runoff event scale, which can provide additional insight into mechanisms of streamflow generation and solute transport at the catchment scale (Li et al., 2022; Minaudo et al., 2019; Musolff et al., 2021). Especially in karst catchment, the event-scale C-Q relationship provides a useful material to assess the spatiotemporal variations in transport processes (Qin et al., 2020; Wang et al., 2020).

Power law equation, in the form $C = aQ^b$, is the most widely used model to describe C-Q relationships of streamflow. According to the coefficients of a and b, C-Q patterns are distinguished into enrichment ($b > 0$), dilution ($b < 0$) and chemostasis pattern ($b \approx 0$), which reflect the change in the solute concentrations versus the corresponding change in discharge (Musolff et al., 2015). Hysteresis occurs when there are differences of concentration for the same discharge during the rising and falling limb of event hydrographs. (Bieroza & Heathwaite, 2015). Which arises as a consequence of mixing of different source water (Zhi & Li, 2020) or difference in the rate at mobilization of sources (Haddadchi & Hicks, 2021). Hysteresis terms are often added to power law formula to consider the hysteresis between concentration and discharge, e. g. $C = aQ^b + c \bullet dQ/dt$ (Minaudo et al., 2017; Musolff et al., 2021; Winter et al., 2021), where coefficient of c describes the hysteresis size (using the absolute value of c) and direction (using the sign of c). Hysteresis directions containing clockwise ($c > 0$) and anticlockwise ($c < 0$) represents the differences in the response rate of concentration and discharge to rainfall. Both the C-Q patterns (enrichment, dilution and chemostasis) and hysteresis (clockwise and anticlockwise) are resulted from the behaviours of solute source mobilization with streamflow changes, controlled by the degree of connection between source and streamflow (Knapp et al., 2022; Stewart et al., 2022). In many studies, it is found that a single power law model usually cannot conform the C-Q relationships from monitoring data across the full wetness range (Minaudo et al., 2019; Moatar et al., 2017). This is not only related to discharge-dependent biogeochemical actions (Moatar et al., 2017), but also to the variations in hydrological connectivity in resource zone (Knapp et al., 2022).

C-Q relationships are related to the source zone distribution in the catchment, and associated hydrological connectivity between them and stream. For example, geogenic species (e.g., Ca, Mg, Si) derived from chemical weathering are usually provided by groundwater (Anderson et al., 1997; Stewart et al., 2022; Zhi et al., 2019), while the soil-enriched species (e.g., rich in carbon-, nitrogen-) are mainly come from shallow soils (Herndon et al., 2015; Pesántez et al., 2018; Tittel et al., 2022). Regardless of the species, catchment hydrological connectivity is the controlling factor of activation of source (Knapp et al., 2020, 2022). Compared with non-karst area, the spatiotemporal variations in hydrological connectivity are more complex in karst area due to the high spatial heterogeneity of critical zone architecture (Zhang et al., 2019). Marked changes in the hydrological connectivity

may occur in a short time (e.g., rising limb of hydrograph) during the runoff event (Al Aamery et al., 2021; Zhang et al., 2021). However, how the changing hydrological connectivity between source zone and stream affects event-scale C-Q relationships in karst catchment remains unclear. In practice, catchment hydrological connectivity cannot be identified by direct observation at the catchment scale. Water age, as a fundamental characteristic of catchment hydrological function, can be used to characterize variations in hydrological connectivity within a hydrological system (Kirchner et al., 2000; McDonnell & Beven, 2014). Which provides an aided index to assess influence of hydrological connectivity on C-Q relationship under different hydrometeorological conditions (Benettin et al., 2017; Soulsby et al., 2015; Sprenger et al., 2019; Zhang et al., 2019).

To help address the general research gaps in solute transport in karst catchment, our overall objective is to better understand variations in C-Q relationships of streamflow in karst catchment and its controls under different hydrometeorological conditions. More specifically in this study, aiming to karst catchment, we sought to address two questions: (1) How do the C-Q relationships of different species in streamflow vary during the runoff event? (2) How does source zone distribution and hydrological connectivity control the intra-event C-Q relationships at the catchment scale?

2 | SITE AND METHODOLOGY

2.1 | Study site

Chenqi catchment (1.25 km^2) is situated in the Puding Karst Ecohydrological Observation Station in Guizhou Province, Southwest China (Figure 1). It is a typical cockpit karst landscape experimental catchment drained by a single underground channel/conduit. This

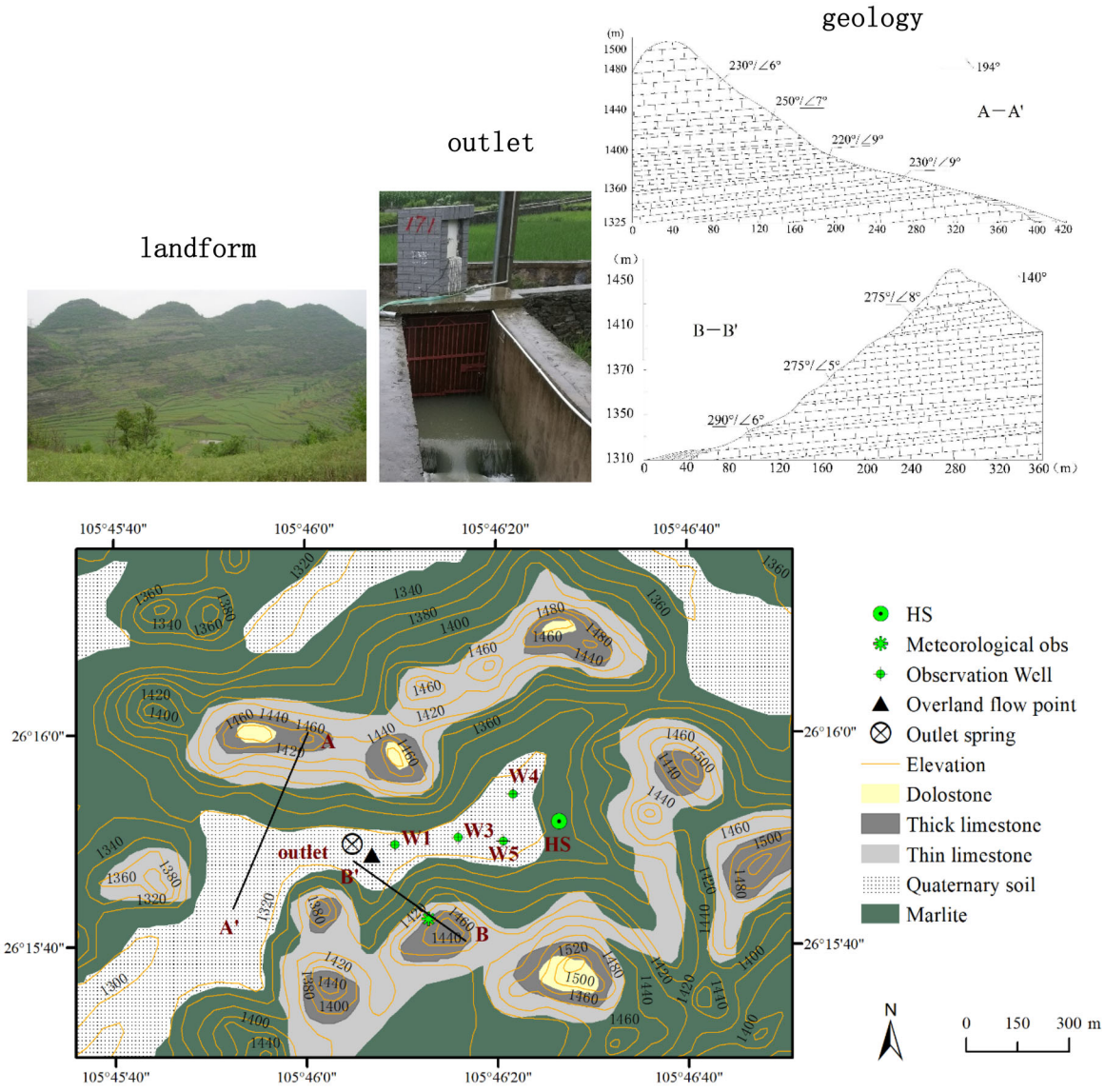

FIGURE 1 Map of the location, geology, geomorphology, hydrological monitoring and sampling locations in the Chenqi catchment.

TABLE 1 Statistics of rainfall and discharges at the catchment outlet and hillslope spring (HS) for the seven events.

		Rainfall (mm)		Discharge (m^3/s)			Modelled flux age (days)		
Event	Date	Amount	Max (mm/h)	Mean	Max	Min	Mean	Max	Min
1	24 Jun	4.4	2.4	0.03	0.065	0.015	142	164	115
2	27 Jun	15.4	2.6	0.05	0.1	0.028	125	147	97
3	30 Jun	51.4	9.6	0.08	0.14	0.03	104	127	82
4	9 Jul	83.4	28.6	0.07	0.15	0.01	81	102	8
5	19 Jul	28	12.2	0.03	0.09	0.003	121	157	21
6	4 Aug	13.6	11.2	0.01	0.05	0.003	134	166	66
7	12 Aug	29.2	16.4	0.03	0.06	0.002	110	186	44

catchment is surrounded by conical hills mainly covered by forest and shrub, separated by star-shaped valley covered by farmland (rice-rape crop rotation). From a 1:10000 digital topography map, the depression area (with elevations <1340 m) and the hillslope area (with elevations of 1340 ~ 1500 m) occupy 0.37 and 0.88 km^2, respectively. In the depression, four observation wells record groundwater table and monitor the hydro-chemical composition (Figure 1). The catchment is subject to a subtropical wet monsoon climate. Mean annual temperature is 20.1°C and mean annual precipitation is ~1140 mm. More than 85% of annual precipitation falls in the wet season from May to September. Geological properties in the catchment are composed of dolostone, thick and thin limestone, marlite and Quaternary soil (cross sections of A–A′ and B–B′ in Figure 1). The limestone with the thickness of 150–200 m is mostly located at higher elevation areas. The marlite underlain the limestone forms an impervious layer and thereby produces karstic springs in this region. The soils overlying the carbonate rocks are thin on the hillslope, with a mean thickness about 30 cm. In depression, soils are relatively thick (over 2 m) and cultivated as cropland.

2.2 | Monitoring, sampling and runoff events selection

The discharges at the catchment outlet and a hillslope spring (HS) located at the foot of the eastern steep hillslope were measured using a v-notch weir instrumented with HOBO U20 water level logger (Onset Corporation). Electrical conductivity (EC) of the catchment outflows was measured in situ with a hydrological chemistry sensor (Aqua TROLL 600 Multiparameter Sonde). The NO_3^- concentrations in catchment outflows were monitored using a non-optical NISE sensor which had been calibrated using the laboratory measurements (Yue et al., 2019). The observation interval for the discharge, EC and NO_3^- concentrations was 15 min during the study period from 12 June and 14 August 2017. There was a meteorological station (Onset HOBO RG3-M) on a southern hillslope (Figure 1), recording precipitation, and temperature in a time interval of 5 min.

Rainfall (at the catchment outlet), flows at catchment outlet and hillslope spring were intensively sampled for using an autosampler setting to hourly intervals during the study periods In this study, groundwater (GW) in the depression mainly came from small fractures (Chen et al., 2018) was sampled from four wells with depth below the ground surface ranging from 13 to 35 m in the depression (Figure 1), for nine times during the study period (Table 1). All water samples were used to analyse ions concentration containing calcium (Ca^{2+}), magnesium (Mg^{2+}), potassium (K^+) and sodium (Na^+). Samples were first stored in high-density polyethylene container and then filtered through 0.45-μm Millipore nitrocellulose membrane filters within 24 h of sampling. The ion concentrations were analysed by inductively coupled plasma optical emission spectrometer, and the analyses were conducted in the Puding Karst Ecohydrological Observation Station within a relative standard deviation (RSD) of 5%.

To explore the C-Q relationship at the event scale, some runoff events during the study period were selected. A separated runoff event in this study was defined as the response of discharge which began with an increase of 10% in a moving window, and ended when discharge decreased less than 0.5% within the moving window or increased again due to another rainfall. According to this division, a total of seven separated events were selected (Figure 2 and Table 1). Sometimes, time interval between two separated runoff events was short, and flow water at the catchment outlet was also collected in some interval between events, for example, a continuous sampling was performed from 21 June to 4 July in this study (Figure 3).

To eliminate the effect of magnitude differences of different solute concentrations, normalized C-Q relationships were used for exploration in this study. The normalized solute concentrations and discharge were estimated as:

$$X_{norm} = (X - X_{min})/(X_{max} - X_{min}), \quad (1)$$

Where, X represents the observed concentrations of a specific solute, X_{min} and X_{max} represent the minimum and maximum concentrations, respectively.

2.3 | Water ages

Tracer-aided hydrological model integrating tracers into rainfall–runoff model allows us to track the water age in streamflow (Hrachowitz et al., 2016; Remondi et al., 2018; Soulsby et al., 2015).

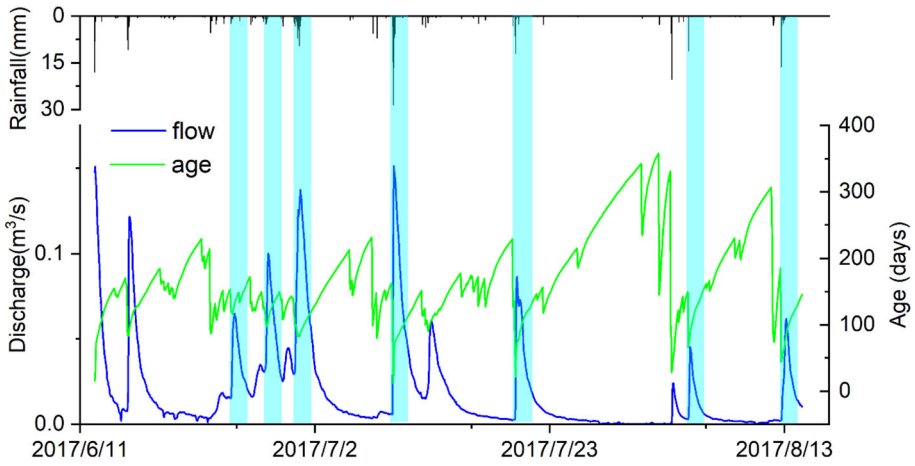

FIGURE 2 Time series of hourly precipitation, discharges and modelled flux ages during the study period, and the seven separated events are highlighted with shaded bars.

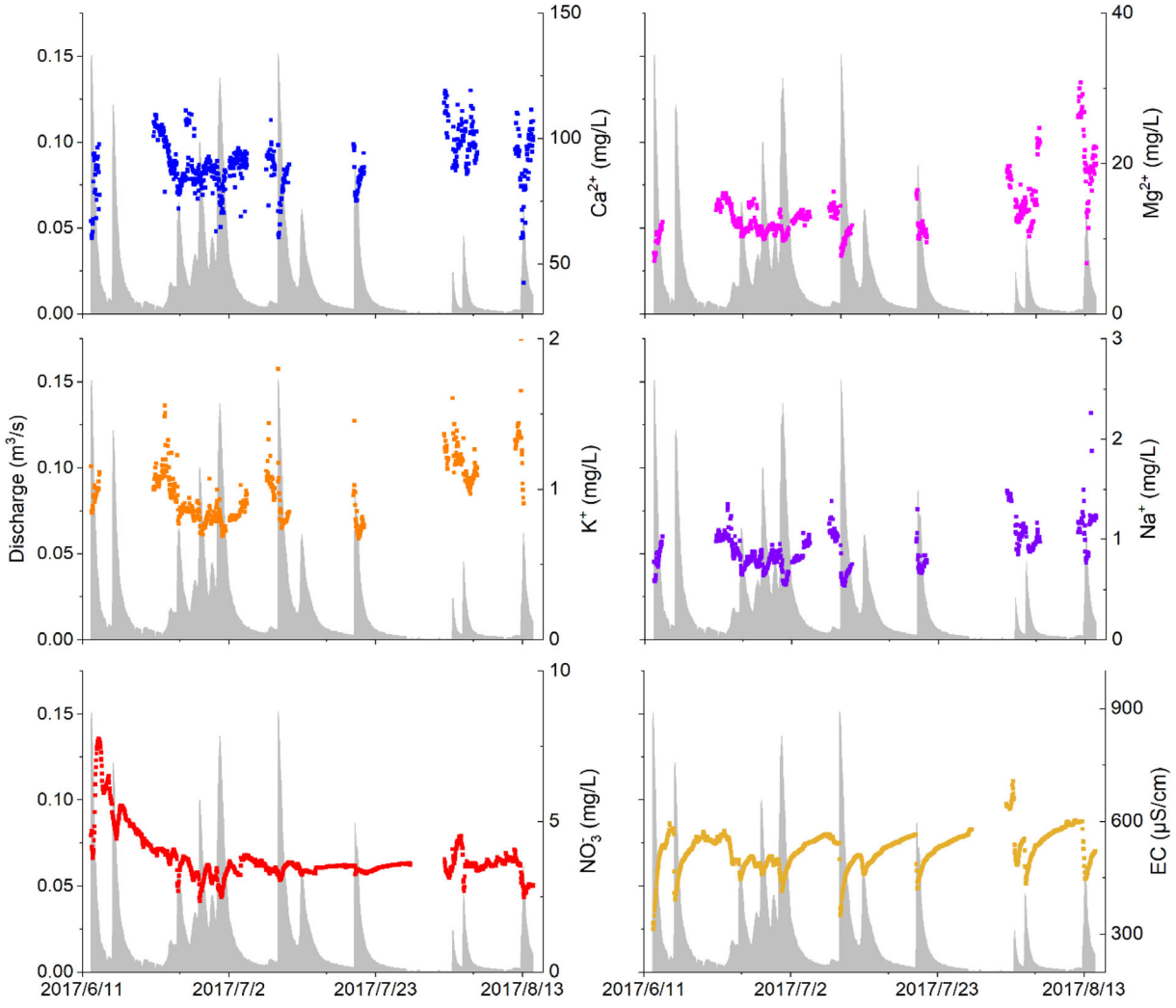

FIGURE 3 Time series of Ca^{2+}, Mg^{2+}, K^{+}, Na^{+}, NO^{-}_{3} and electrical conductivity (EC) during the study period. The shade represents the discharge.

To link water concentrations of dissolved solute to water age, a robust tracer-aided runoff model for karst catchments developed by Zhang et al. (2019) was used to track the flux age in different landscape units. The model consisted of two main conceptual stores representing the main landscape units: the hillslopes and the depression. To conceptualize the typical dual-flow system of the karst critical zone (Hartmann et al., 2014), the depression store was subdivided into slow and fast reservoirs. Which represent the low-permeability

TABLE 2 Statistics of solute concentrations and electrical conductivity (EC) in catchment outflows for the seven events.

Event	Concentration (mg/L) and EC (μS/cm)					
	Ca^{2+}	Mg^{2+}	K^{+}	Na^{+}	NO_3^{-}	EC
1	85 ± 9	11.6 ± 1.2	0.9 ± 0.1	0.8 ± 0.1	3.52 ± 0.34	476 ± 17
2	85 ± 4	10.9 ± 0.5	0.8 ± 0.06	0.7 ± 0.07	2.95 ± 0.29	477 ± 11
3	80 ± 6	11.1 ± 1.2	0.8 ± 0.08	0.7 ± 0.1	2.99 ± 0.31	462 ± 25
4	79 ± 9	10.2 ± 1.3	0.9 ± 0.2	0.7 ± 0.08	3.25 ± 0.14	419 ± 40
5	85 ± 6	11.7 ± 1.8	0.8 ± 0.1	0.8 ± 0.1	3.35 ± 0.07	496 ± 34
6	98 ± 7	15.9 ± 4.2	1.1 ± 0.07	1 ± 0.07	3.48 ± 0.25	508 ± 32
7	87 ± 15	19 ± 4.1	1.3 ± 0.3	1.1 ± 0.3	2.91 ± 0.26	504 ± 43

media, for example, primary porosity in the matrix blocks and small fractures in the aquifer, and the large fractures and conduits with a high permeability, respectively. By conceptualizing the hydrological connectivity of the catchment that links the conceptual stores, this tracer-aided model successfully captured the nonlinear flow response in karst catchment. By tracking the input and output fluxes with isotope fingerprints through each conceptual store, the flux ages of different landscape units could be estimated. A complete mixing was assumed for both slow and fast reservoirs in the depression unit, and an active reservoir with an additional passive reservoir only for the tracer mixing simulation is employed to estimate the water and tracer dynamics in the hillslope unit. The flux ages of the catchment outlet flows were estimated by integrating the contribution of water flux from each conceptual store with different ages. Model calibration and verification have been performed using hourly flow discharge and stable isotopes at outlet, hillslope spring and groundwater in the wells in the study catchment. Please refer to Zhang et al. (2019) for full details of how the water ages were derived.

3 | RESULTS

3.1 | Dynamics of discharge, water age and solute concentration

The total precipitation amount was 437 mm over the study period from 12 June to 14 August 2017, with the maximum rainfall intensity of 28.6 mm per hour. For the study period, the mean discharges were 0.019 and 0.27 $\times$ 10^{-3} m^3/s, and the median flow ages derived from the tracer-aided model were 154 and 109 days at the catchment outlet and HS, respectively (Figure 2). Figure 3 showed the dynamics of solute concentrations in catchment outlet flows. The concentrations of Ca^{2+} and Mg^{2+} were at a relatively high level during the study period, with the means of 90 and 13.6 mg/L, which is similar to monitoring in many other studies in carbonate-rich catchment with strong rock weathering (Qin et al., 2020; Zhong et al., 2018). The mean concentrations of K^{+}, Na^{+} and NO_3^{-} were 0.97, 0.90 and 3.86 mg/L, respectively. The mean EC was 537 μS/cm over the study period.

For the seven selected runoff events, the means of rainfall, discharge and modelled flow age at catchment outlet ranged from 4.4 to 83.4 cm, 0.01 to 0.08m^3/s and 81 to 142 days, respectively (Table 1). The largest discharge was 0.15 m^3/s for the event on 9 July with the largest rainfall intensity of 28.6 mm per hour. The lowest flow age was ~8 days corresponding to the largest discharge. For the seven events, the mean concentrations of Ca^{2+}, Mg^{2+}, K^{+}, Na^{+}, NO_3^{-} and EC in catchment outflows ranged from 79 to 98 mg/L, 10.2 to 19 mg/L, 0.8 to 1.3 mg/L, 0.7 to 1.1 mg/L, 2.95 to 3.52 mg/L and 419 to 508 μS/cm, respectively (Table 2).

3.2 | End-member source waters of the catchment outflows

In this study, the catchment was drained by an underground conduit, hence, the catchment outflows were treated as conduit flows. Which were derived primarily from three sources with distinct chemical characteristics: hillslope flows, diffuse recharges resemble water in small fractures and concentrated recharges via large fractures or sinkholes (Hartmann et al., 2014). The concentrated recharges usually come from lateral flow at the surface after rain, i.e. overland flows. In this study, hillslope flows were sampled from the hillslope spring, diffuse recharges from wells in depression (referred to as groundwater below) mainly collecting small fracture waters, concentrated recharges from overland flow point at surface in the depression (Figure 1). Figure 4 showed the solute concentration and EC in different end-member water sources, and the values of NO_3^{-} concentration and EC in overland flow and groundwater came from the research by Tan (2020). The results showed that the highest concentrations of K^{+} and NO_3^{-} (classified as the soil-enriched solutes) were in overland flow, with the means of 3.5 and 19.8 mg/L, respectively. This was consistent with the findings by Wang et al. (2020). In this area, the nutrients (e.g., nitrogen, phosphorus and potassium) are mostly accumulated in the soils, which come from the fertilization in the depression with the light fertilization for rape in October–November, and the heavy fertilization for rice in May–early June (Yue et al., 2019). According to mineral composition test using XRD, Dmax-IIIa, Japan, Wang (2008) reported that 75% of the surface soils consists of illite-smectite mixed mineral with high potassium. Hence, the surface soil is the main

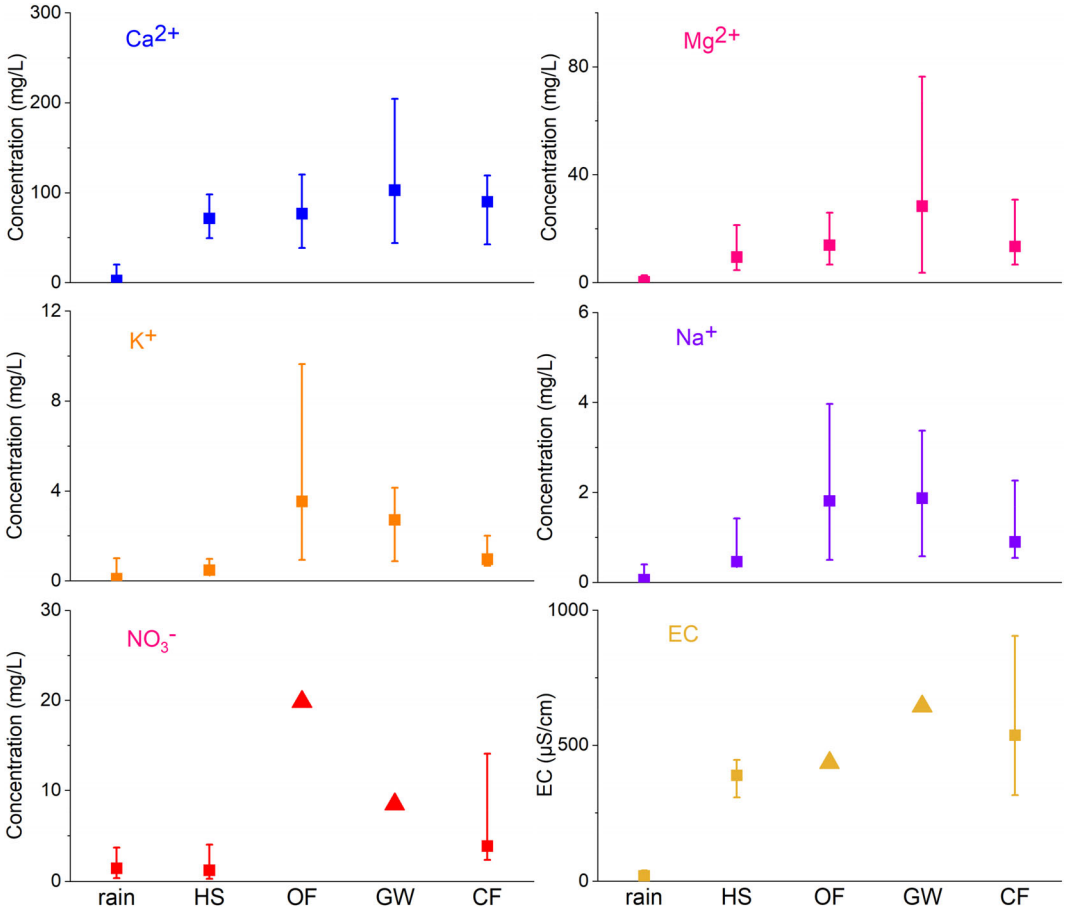

FIGURE 4 Solute concentration in rain, hillslope flow, overland flow, groundwater, and conduit flow ($p < 0.05$). The triangles represent the mean values from Tan (2020). CF, conduit flow; GW, groundwater; HS, hillslope water; OF, overland flow.

source zone of K^+ and NO_3^- in conduit flow. It is worth noting that the concentrations of K^+ and NO_3^- in groundwater in the depression (2.7 and 8.46 mg/L, respectively) were higher than that in conduit flow. Which reveals that the small fractures in depression could be another minor source zone of K^+ and NO_3^- in conduit flows. The concentrations of Na^+ were higher both in overland flows and groundwater (1.87 and 1.81 mg/L) than that in conduit flows (0.9 mg/L), which was treated as a soil enriched solute in this study. By contrast, the highest concentrations of Ca^{2+} and Mg^{2+}, classified as the geogenic solutes (Zhi et al., 2019), were in groundwater with the means of 103.3 and 37.1 mg/L, respectively. Which indicated that the small fractures are the main source zone for Ca^{2+} and Mg^{2+} in conduit flows (with the mean values of 90 and 13.6 mg/L, respectively).

Chemical weathering of various rocks, as well as atmospheric and anthropogenic inputs, are main contributors of dissolved loads in streamflow (Gaillardet et al., 1999). Many previous studies have confirmed that the chemical weathering of rocks, especially the carbonate weathering, has a controlling effect on concentration of geogenic solutes (e.g., Ca, Mg) in streamflow in karst area (Zhong et al., 2017). The Na normalized molar ratios of Mg^{2+}/Na^+ and Ca^{2+}/Na^+ in the dissolved phase of streamflow can be used to characterize the weathering of silicate, carbonate and evaporite at

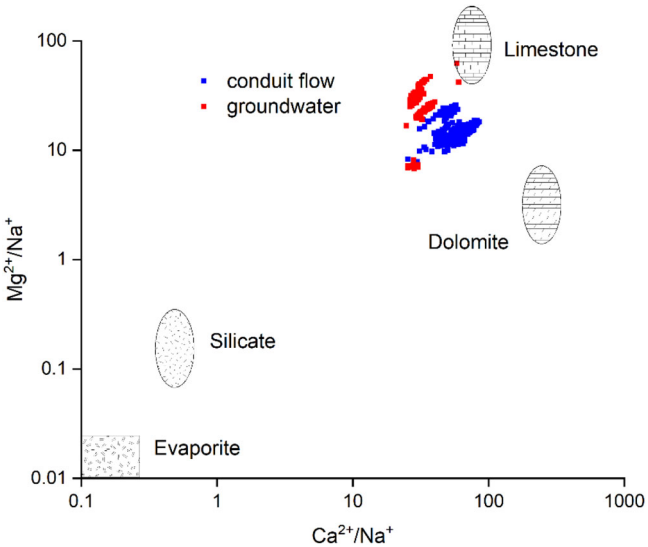

FIGURE 5 The relationships of Mg^{2+}/Na^+ versus Ca^{2+}/Na^+ in conduit flows and groundwater in the depression.

catchment scale (Gaillardet et al., 1999). The relationships of Mg^{2+}/Na^+ versus Ca^{2+}/Na^+ in conduit flow and groundwater in the depression for Chenqi catchment were shown in Figure 5. The

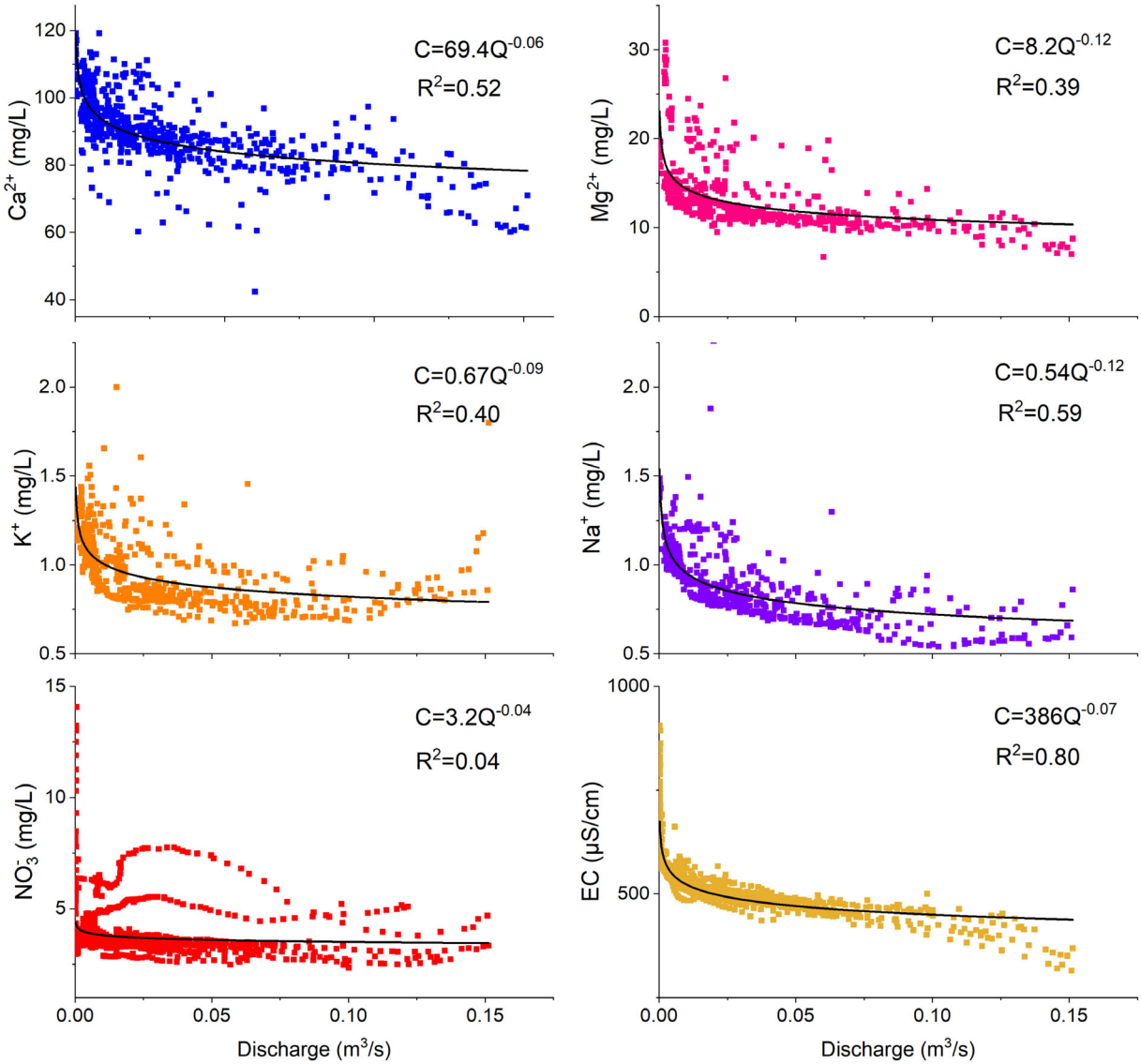

FIGURE 6 Power-law relationships between concentration and discharge over the whole study period for each solute.

results showed the marked high values of Ca^{2+}/Na^{+}, indicating the strong limestone weathering. This is consistent with the findings by Wang (2008) that the geologic stratum of this catchment is predominantly calcite rich rocks. Compared to groundwater in the depression with long residence time, the water from hillslope has relatively short resistance times (a mean age of ~109 days by Zhang et al. (2021)), which weakens the rock weathering. In addition, the thin soil layer on hillslope results in relatively little soil carbon dioxide dissolution (Li & Li, 2018), which limits the weathering of carbonate in hillslope. Therefore, the concentrations of Ca^{2+} and Mg^{2+} were relatively low in hillslope flow, with the mean values of 75 and 9.5 mg/L, respectively (Figure 4).

The mass of Ca^{2+} and Mg^{2+} accounting for over 90% of the cations in conduit flow (Tan, 2020), resulting in the highest EC in groundwater with the mean of 644 µS/cm, which indicated that the small fracture was the main 'source zone' of EC in conduit flows.

3.3 | C-Q behaviours of different solutes in conduit flow

Figure 6 showed the general C-Q relationships of Ca^{2+}, Mg^{2+}, K^{+}, Na^{+}, NO_3^{-} and EC in conduit flows over the study period. The results indicated that C-Q relationships of these solutes can be generally described by a power law model in the form $C = aQ^{b}$. The negative *b* indicated a dilution C-Q pattern for all constituents during the study period. It was notable that the variations in the concentration of NO_3^{-} were more complex than the other solutes, which could be associated with the biogeochemical reaction of nitrate.

The dynamics of hourly discharge, water age and solute concentration for each separated event were shown in Figure 7. Here is the case of event No. 1 on 9 July 2017, and the results for the other events are in Data S1. During the event, the modelled ages of conduit flow declined and then increased. The lowest water age appeared

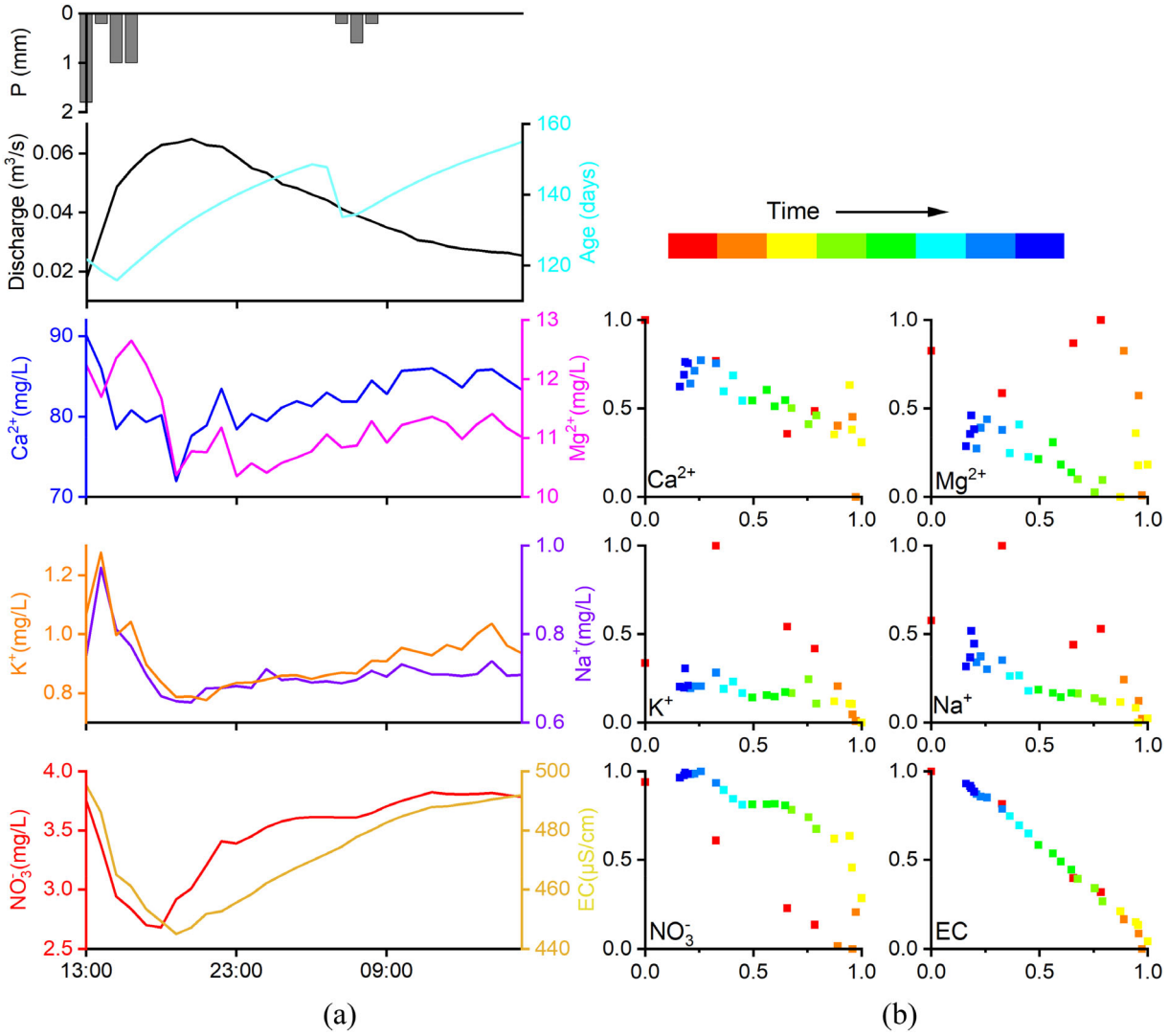

FIGURE 7 (a) Dynamics of hourly discharge, modelled flow age and solute concentration in conduit flows for the event on 24 June 2017 (event No. 1 in Table 1); (b) the normalized C-Q behaviours of solutes.

earlier than the flow peak, which indicated the rapid entrance of young water at the beginning of the event. There was a little decline of conduit flow age at 5 o'clock 25 June, on the falling limb of hydrograph, which was due to a small rainfall (with the rainfall amount less than 1 mm). The concentrations of Ca^{2+}, Mg^{2+}, NO_3^- and EC in conduit flow decreased with the increase of discharge on the rising limb, and then increased gradually on the falling limb. The concentration curves of these solutes showed a general shape of letter 'V' during the event, which indicated the dilution C-Q pattern over the entire event (Figure 7b). The C-Q relationship of Mg^{2+} showed chaotic variations on the rising limb in this event, which may be related to the antecedent concentration conditions in the catchment. In contrast, the concentrations of K^+ and Na^+ increased first (increased by ~33% and 27% in the first hour, respectively) and then decreased (Figure 7a) on the rising limb, and gradually increased on the falling limb. During the event, the concentration curves of K^+ and Na^+ showed a shape of letter 'N' with two inflection points. Which indicated that the C-Q patterns changed from enrichment to dilution during the event (Figure 7b).

The difference of C-Q patterns for different species mainly occurred in the early of event (Figure 7). Here, the ratio of percentage changes in solute concentration and discharge, at the first hour of each event, was estimated as: $\Delta Q = (Q_n - Q_0)/Q_0 \times 100\%$; $\Delta C = (C_n - C_0)/C_0 \times 100\%$. Where, Q and C represent discharge and concentration, and the subscript 0 and n represent the start time and elapsed time ($n = 1$ in this study) for the runoff event, respectively. The results show that the percentage changes in discharge at the first hour ranged from 13% to 291% (with the mean of 87%) for the seven events. The concentration of Ca^{2+} tended to decrease at the first hour, and its percentage changes ranged from −0.6% to −27.1% for the seven events, which indicated the dilution C-Q pattern at the beginning of the event. On the contrary, the concentration of K^+ increased at the

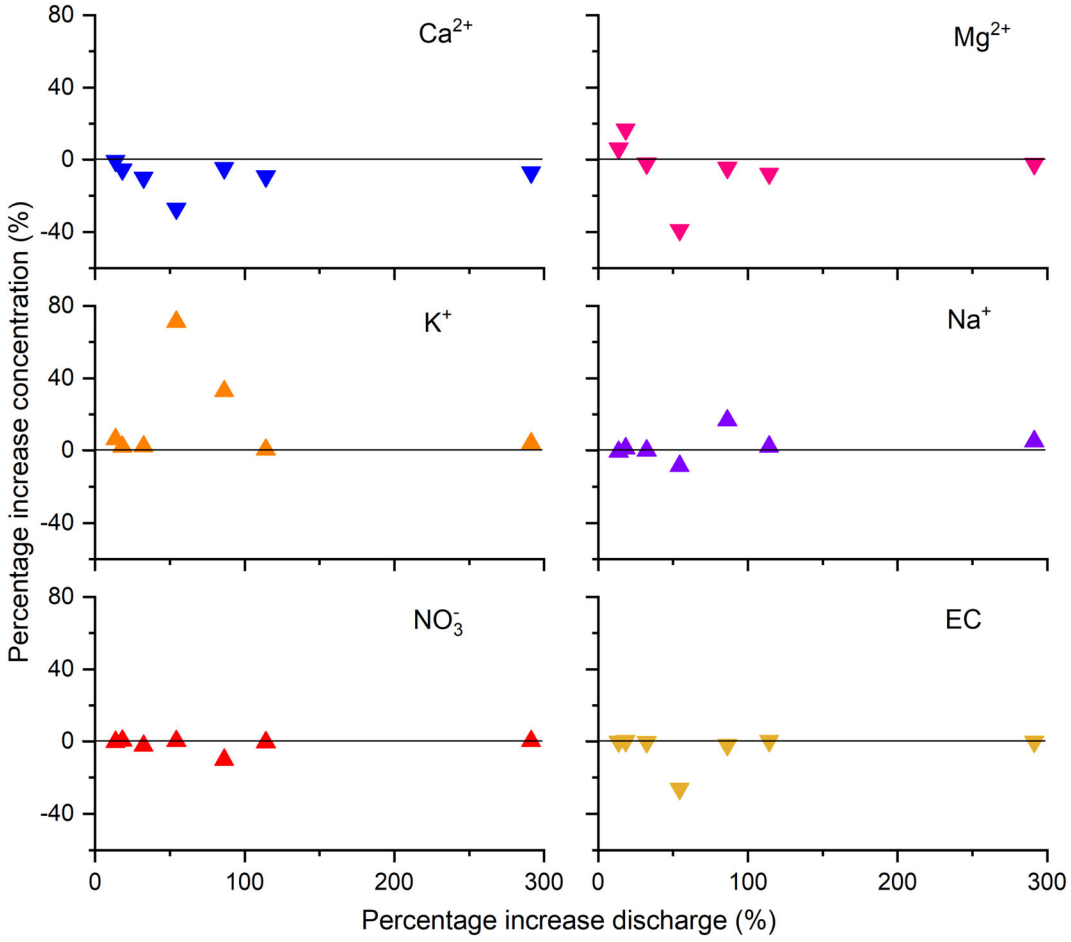

FIGURE 8 Percentage changes in the solute concentration at the first hour of each event versus the corresponding percentage changes in discharge.

first hour for all events, with the percentage changes from 0.4% to 71.3% (Figure 8), indicating an enrichment C-Q pattern. The percentage changes in concentrations of Mg^{2+} and EC increased in most events while decreased in some others (Figure 8), and the percentage changes in Na^{+} and NO_3^{-} concentrations showed irregular changes at the first hour of event.

3.4 | Empirical models for intra-event C-Q relationship

There were significant changes in C-Q relationships during the runoff event (Figure 7). To consider the variations and associated influence factors, we used piecewise models to fit the C-Q patterns on rising and falling limb, respectively, instead of single model with constant coefficients for a whole event (Musolff et al., 2021; Qin et al., 2020; Winter et al., 2021). The negative C-Q relationships for geogenic solutes (e.g., Ca^{2+} and Mg^{2+}) showed dilution patterns on both rising and falling limbs. Here, two power law equations, in the form of $C = aQ^b$, with different coefficients were chosen for the rising and falling limbs, respectively. Taking the C-Q behaviours of Ca^{2+} of event No. 1 on 24 June 2017 as an example (Figure 9), the results showed that these two power law formulations can capture the C-Q behaviours on both sides of the hydrograph, with R^2 of 0.77 and 0.65, respectively. The values of b, representing the C-Q slopes in log–log space, for the rising limb (−0.13) were lower than that for the falling limb (−0.07). Which indicated an exhaustible, proximal source of groundwater on the rising limb. It can be inferred that the piecewise fitting models can be used to explore variations in contributions of different source water or activations of solute sources during the event, which are usually identified through hysteresis analysis (Li et al., 2022; Lloyd et al., 2016).

Due to theoretical monotonicity, power-law models cannot describe the changes in C-Q patterns from enrichment to dilution for K^{+} (Figure 9). In this study, a parabolic equation in the form of $ax^2 + bx + c$ was used to fit the C-Q pattern of K^{+} on the rising limb of hydrograph. The results showed that the C-Q relationship can be captured well on the rising side of hydrograph, with R^2 of 0.92. The positive C-Q relationship (enrichment pattern) implied that the proximal source of K^{+} was plentiful at the beginning of the rising phase. Then supply limitation occurred and the C-Q pattern reversed in the later of rising limb. On the falling limb, the concentrations increased

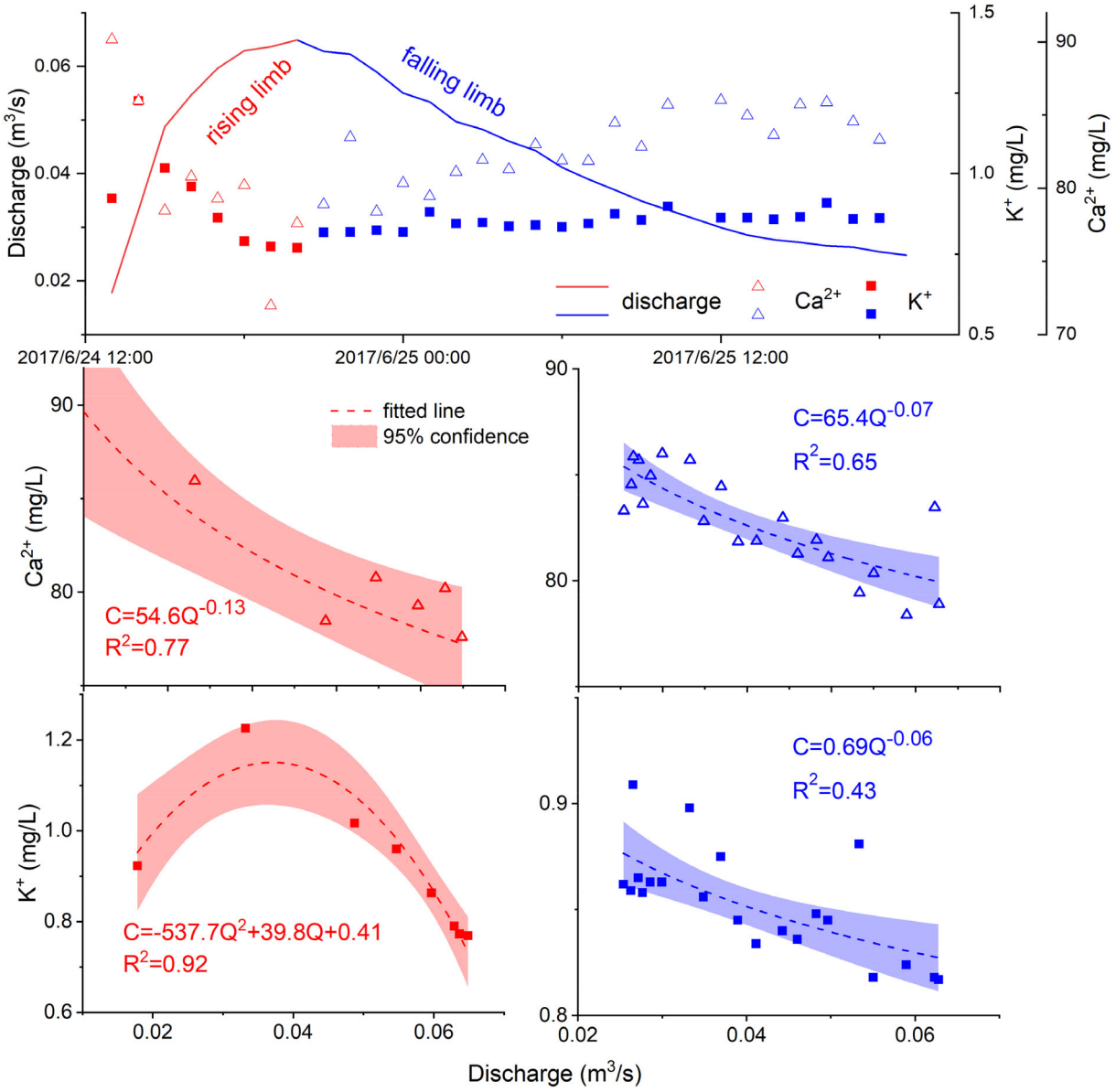

FIGURE 9 C-Q relationships (Ca^{2+} and K^{+}) at the rising and falling limbs of hydrograph for the event on 24 June 2017.

monotonically with the decrease of discharge, showing a dilution C-Q pattern. Thus, a power law equation was used to fit the C-Q relationship on this limb, and the model can generally capture the C-Q relationship, with R^2 of 0.43. It worth noting that the K^{+} has a similar dilution C-Q pattern to Ca^{2+} on the falling limb of the hydrograph, which revealed that they have the same source water, that is, groundwater, during this phase. According to the variations in concentrations and discharges in Figure 7, it can be found that not all soil-enriched solutes follow the same C-Q pattern as K^{+} during the event, for example, NO_3^{-}. The most likely explanation relates to the biogeochemical reactions and anthropic impacts on the solute fates at the catchment scale. This is consistent with findings in many studies that some soil-enriched solutes usually show different C-Q relationships at the event scale (Liu et al., 2022).

4 | DISCUSSION

4.1 | Constraint of hydrological connectivity on inter-event C-Q patterns

Geogenic solutes usually exhibit high concentrations in groundwater due to mineral weathering upon long-time contact between water and rocks (Ameli et al., 2017; Rose et al., 2018). According to ion monitoring in this study, the concentrations of geogenic solutes in overland flows in depression and hillslope flows were lower than that in the conduit flows (Figure 4). In other words, groundwater is the main source of geogenic solutes in stream/under river flows (Zeng et al., 2019). On the rising limb of hydrograph, the decrease trend of concentrations of geogenic solutes (e.g., Ca and Mg) in conduit flows

indicated the entrance of water with low concentrations. The increase of overland and hillslope flow contributions can cause this dilution C-Q pattern. Water age can provide information to exactly identify the source water for this C-Q behaviours. Conduit flow ages dropped rapidly from a few hundred days to a dozen days at the beginning of rainfall (Figure 2), while the ages of hillslope flows were about 100 days (with mean of ~109 days) during the same period (Zhang et al., 2019). Hence, it can be inferred from the dynamics of water age that the dilution C-Q pattern of geogenic solute in the early of rising limb was caused by the high contribution of overland flows with low age (Zhang et al., 2021). This was related to the strengthening hydrological connectivity between surface and conduit through large fractures or sinkholes in depression at the early of runoff event. With the strengthening of hydrological connectivity between hillslope and depression, the contribution of hillslope flows to conduit flows increased in the later of rising limb. Which resulted in the continuous dilution C-Q pattern during this phase. The flatter C-Q slope on the falling limb indicated the gradual dominant of groundwater with higher availability of solutes in contrast to overland and hillslope flows. The increasing ages of conduit flow on the falling limb supported this hypothesis (Figure 7a).

In no-karst area, many researches found that C-Q slopes of geogenic solutes were usually invariant during runoff event, due to the relatively constant contribution of groundwater to streamflow (Anderson et al., 1997; Godsey et al., 2009; Stewart et al., 2022). Which indicated the hydrologic connectivity had less effect on variations in C-Q slope (Knapp et al., 2020). However, hydrological connectivity between small fractures (slow flow system) and conduit (fast flow system) showed significant variation across wetness states in karst area (Chen et al., 2018; Wang et al., 2022). Which can result in the changes in C-Q slopes during runoff event, as the contributions of groundwater changes with hydrological connectivity. Therefore, time-variant models could be needed for C-Q relationship fitting in karst catchment with rapid variability of hydrological connectivity during the event.

For soil-enriched solutes, diffuse percolation of soil water to small fractures in depression increases the availability of solutes in small fracture water (Sorensen et al., 2015; Yue et al., 2019). In addition, higher water level in conduits at the beginning of a flood can lead water flux with high concentrations (showing in Figure 7) from conduits to small fractures, known as the 'bidirectional exchange' between conduit and small fracture in karst critical zone (Chen et al., 2018; Zhang et al., 2017). These make the small fractures in epikarst a secondary source zone for soil-enriched solutes in conduit flows, and the monitoring results of concentration (Figure 4) approved our hypothesis. Therefore, both overland flows and groundwater in depression, in theory, could produce the increases of solute concentrations at the beginning of rising limb, as well as falling limb phases (Figure 7). Fortunately, water age provides information to determine the mixing of different water sources with a different timing (Botter, 2012; van der Velde et al., 2015), which can be used to identify which source is mobilized at different wetness stages. According to variations in water ages, the strong hydrological connectivity between surface and subsurface mobilizing the source of soil layer in the depression, because the sharp increase of concentrations with the increase in discharge (the enrichment C-Q pattern) at the beginning of rising limb. On the contrary, the dominant of groundwater in the conduit flows results in the gradual increase of concentrations with the decrease in discharge (the dilution C-Q pattern) on the falling limb. At the later of rising limb, the ages of conduit flows indicated the strong hydrological connectivity between hillslope and depression (Zhang & Shao, 2018), which causes C-Q pattern convert from enrichment to dilution due to the entrance of hillslope flows with low concentrate. Hence, it can be deduced that affected by multiple sources and the variations in hydrological connectivity under different wetness conditions, the C-Q relationships of K^+ show an 'enrichment- dilution- dilution' pattern (Figure S2), which correspond with the 'N' dynamics of concentrations during the runoff event.

It is worth to note that the soil enriched solutes, for example, K^+ or NO_3^- in this study are related to the anthropic actions (Lorette et al., 2022; Yang et al., 2020). Therefore, they are mainly concentrated in the soil and small fractures in the depression, but very low in the hillslope unit. However, some other soil-enriched solutes, for example, soluble carbon have significant high concentrations on hillslope in karst catchment (Liu et al., 2023), and they could have different C-Q behaviours under different wetness during the runoff event.

4.2 | Broader implications of C-Q relationships on agricultural management in the karst catchment

About one-third of global fertilizers is used in China for agriculture (Ju et al., 2009; Wang et al., 2020), and the relatively low efficiency of fertilizer use leads the risk of water quality deterioration, particularly in karst area of southwest of China, one of the most ecologically fragile regions in China (Tan et al., 2015). For example, fertilizer application is growing by 3.5% each year from 1996 to 2015 in Guizhou province, the centre of Yunnan-Guizhou Plateau of southwest China (one of the largest, continuous karst areas in the world). The mean utilization rate of fertilizer in Guizhou (587.98 kg/hm^2) was 1.32 times that of China (446.12 kg/hm^2). The intensive fertilizer application in agriculture in karst area increases the concentration of solutes in soil. Meanwhile, it leads potential nutrient losing and aquifer contamination under the rapid hydrological condition, especially during heavy rainfall events (Yue et al., 2020). The enrichment C-Q pattern of soil enriched solutes, for example, K^+, could cause the solutes losing and aquifer contamination at the beginning of storm. Some of the pollutants from soils may absorbed by small fractures in the depression during runoff events due to the 'bidirectional exchange' between ground conduits and small fractures, as well as the diffuse infiltrations. During dry period, this source zone, as a 'hotspot' of contaminant, will release the water with high solute concentrations. According to observation by Puding Karst Ecohydrological Observation Station in China, the concentration of K^+ in well water is still in a high level during dry season, with the mean value of 2.4 ± 1 mg/L. Which means the removal of dissolved solutes stored in the slow flow system will be a

long process in karst aquifer in depression. Hence, in addition to reducing utilization rate of fertilizer, appropriate fertilizer should be selected to inhibit solute accumulation in soil. Avoidances of fertilization before storm and near to uncovered fractures or sinkholes are also a potential requirement of agricultural management in karst area.

5 | CONCLUSION

In this study, we explored the intra-event C-Q relationships of different solutes and its variations with the changes in hydrological connectivity in karst catchment, by integrating solute concentration, discharge and water age tracked by a calibrated karstic tracer-aided model in a 1.25 km^2 karst catchment in southwest China. Generally, geogenic solutes showed the dilution C-Q patterns during the runoff event, and the piecewise power-law formulations can describe the C-Q patterns on both rising and falling limb of hydrograph. Variations in hydrological connectivity between surface, hillslope and conduits leaded significant differences in the dilution C-Q patterns at different phrases of event, which revealed the changes in mobilization mechanisms during the runoff event. Both soil layer and small fractures in the depression were source zones of soil-enriched solutes. However, mobilizations of solutes in these two sources affected by hydrological connectivity could result in different C-Q patterns under different wetness conditions. As a result, there was a notable change in C-Q patterns from enrichment to dilution during the runoff event. In this study, we highlighted the effects of water ages in identifying the water sources and flow paths in the karst catchment. In addition, piecewise models could be needed to capture the variations in C-Q relationships during the runoff event. In future work, more and longer observations of chemistry of various end-member source water are needed for assessment and testing the hypothesises of solute transport in karst catchment. Assessing the influence of biogeochemical processes on C-Q relationship in streamflow is also requested.

ACKNOWLEDGEMENTS

This research was supported by the National Natural Science Foundation of China (42030506, 41971028, 42071039).

DATA AVAILABILITY STATEMENT

The data that support the findings of this study are available from the corresponding author upon reasonable request.

ORCID

Zhicai Zhang https://orcid.org/0000-0003-1146-6685
Xi Chen https://orcid.org/0000-0003-3647-5617
Siliang Li https://orcid.org/0000-0002-0295-9675
Fujun Yue https://orcid.org/0000-0003-3733-7216

REFERENCES

Al Aamery, N., Adams, E., Fox, J., Husic, A., Zhu, J., Gerlitz, M., Agouridis, C., & Bettel, L. (2021). Numerical model development for investigating hydrologic pathways in shallow fluviokarst. *Journal of Hydrology*, *593*, 125844. https://doi.org/10.1016/j.jhydrol.2020.125844

Ameli, A. A., Beven, K., Erlandsson, M., Creed, I. F., McDonnell, J. J., & Bishop, K. (2017). Primary weathering rates, water transit times, and concentration-discharge relations: A theoretical analysis for the critical zone. *Water Resources Research*, *53*(1), 942–960. https://doi.org/10.1002/2016WR019448

Anderson, S. P., Dietrich, W. E., Torres, R., Montgomery, D. R., & Loague, K. (1997). Concentration-discharge relationships in runoff from a steep, unchanneled catchment. *Water Resources Research*, *33*(1), 211–225. https://doi.org/10.1029/96WR02715

Bakalowicz, M. (2005). Karst groundwater: A challenge for new resources. *Hydrogeology Journal*, *13*(1), 148–160. https://doi.org/10.1007/s10040-004-0402-9

Basu, N. B., Thompson, S. E., & Rao, P. S. C. (2011). Hydrologic and biogeochemical functioning of intensively managed catchments: A synthesis of top-down analyses. *Water Resources Research*, *47*(10), 10800. https://doi.org/10.1029/2011WR010800

Benettin, P., Soulsby, C., Birkel, C., Tetzlaff, D., Botter, G., & Rinaldo, A. (2017). Using SAS functions and high-resolution isotope data to unravel travel time distributions in headwater catchments. *Water Resources Research*, *53*(3), 1864–1878. https://doi.org/10.1002/2016WR020117

Benischke, R. (2021). Review: Advances in the methodology and application of tracing in karst aquifers. *Hydrogeology Journal*, *29*(1), 67–88. https://doi.org/10.1007/s10040-020-02278-9

Berglund, J. L., Toran, L., & Herman, E. K. (2019). Deducing flow path mixing by storm-induced bulk chemistry and REE variations in two karst springs: With trends like these who needs anomalies? *Journal of Hydrology*, *571*, 349–364. https://doi.org/10.1016/j.jhydrol.2019.01.050

Bieroza, M. Z., & Heathwaite, A. L. (2015). Seasonal variation in phosphorus concentration–discharge hysteresis inferred from high-frequency in situ monitoring. *Journal of Hydrology*, *524*, 333–347. https://doi.org/10.1016/j.jhydrol.2015.02.036

Botter, G. (2012). Catchment mixing processes and travel time distributions. *Water Resources Research*, *48*, 5. https://doi.org/10.1029/2011WR011160

Buckerfield, S. J., Waldron, S., Quilliam, R. S., Naylor, L. A., Li, S., & Oliver, D. M. (2019). How can we improve understanding of faecal indicator dynamics in karst systems under changing climatic, population, and land use stressors? – Research opportunities in SW China. *Science of the Total Environment*, *646*, 438–447. https://doi.org/10.1016/j.scitotenv.2018.07.292

Chen, X., Zhang, Z., Soulsby, C., Cheng, Q., Binley, A., Jiang, R., & Tao, M. (2018). Characterizing the heterogeneity of karst critical zone and its hydrological function: An integrated approach. *Hydrological Processes*, *32*(19), 2932–2946. https://doi.org/10.1002/hyp.13232

Dupas, R., Jomaa, S., Musolff, A., Borchardt, D., & Rode, M. (2016). Disentangling the influence of hydroclimatic patterns and agricultural management on river nitrate dynamics from sub-hourly to decadal time scales. *Science of the Total Environment*, *571*, 791–800. https://doi.org/10.1016/j.scitotenv.2016.07.053

Ford, D., & Williams, P. (2013). *Karst hydrogeology and geomorphology*. John Wiley & Sons. https://doi.org/10.1002/9781118684986

Ford, W. I., Husic, A., Fogle, A., & Taraba, J. (2019). Long-term assessment of nutrient flow pathway dynamics and in-stream fate in a temperate karst agroecosystem watershed. *Hydrological Processes*, *33*(11), 1610–1628. https://doi.org/10.1002/hyp.13427

Gaillardet, J., Dupré, B., Louvat, P., & Allègre, C. J. (1999). Global silicate weathering and CO2 consumption rates deduced from the chemistry of large rivers. *Chemical Geology*, *159*(1–4), 3–30. https://doi.org/10.1016/S0009-2541(99)00031-5

Godsey, S. E., Kirchner, J. W., & Clow, D. W. (2009). Concentration-discharge relationships reflect chemostatic characteristics of US

catchments. *Hydrological Processes*, *23*(13), 1844–1864. https://doi.org/10.1002/hyp.7315

Haddadchi, A., & Hicks, M. (2021). Interpreting event-based suspended sediment concentration and flow hysteresis patterns. *Journal of Soils and Sediments*, *21*(1), 592–612. https://doi.org/10.1007/s11368-020-02777-y

Hao, Z., Gao, Y., Ma, M., Green, S. M., Wang, J., Song, X., Dungait, J. A. J., Johnes, P. J., Xiong, B., Quine, T. A., Sun, X., Wen, X., & He, N. (2019). Using δ13C to reveal the importance of different water transport pathways in two nested karst basins, Southwest China. *Journal of Hydrology*, *571*, 425–436. https://doi.org/10.1016/j.jhydrol.2019.01.070

Hartmann, A., Goldscheider, N., Wagener, T., Lange, J., & Weiler, M. (2014). Karst water resources in a changing world: Review of hydrological modeling approaches. *Reviews of Geophysics*, *52*(3), 218–242. https://doi.org/10.1002/2013RG000443

Herndon, E. M., Dere, A. L., Sullivan, P. L., Norris, D., Reynolds, B., & Brantley, S. L. (2015). Landscape heterogeneity drives contrasting concentration–discharge relationships in shale headwater catchments. *Hydrology and Earth System Sciences*, *19*(8), 3333–3347. https://doi.org/10.5194/hess-19-3333-2015

Herndon, E. M., Steinhoefel, G., Dere, A. L. D., & Sullivan, P. L. (2018). Perennial flow through convergent hillslopes explains chemodynamic solute behavior in a shale headwater catchment. *Chemical Geology*, *493*, 413–425. https://doi.org/10.1016/j.chemgeo.2018.06.019

Hoagland, B., Russo, T. A., Gu, X., Hill, L., Kaye, J., Forsythe, B., & Brantley, S. L. (2017). Hyporheic zone influences on concentration-discharge relationships in a headwater sandstone stream. *Water Resources Research*, *53*(6), 4643–4667. https://doi.org/10.1002/2016WR019717

Hrachowitz, M., Benettin, P., van Breukelen, B. M., Fovet, O., Howden, N. J. K., Ruiz, L., van der Velde, Y., & Wade, A. J. (2016). Transit times-the link between hydrology and water quality at the catchment scale. *Wiley Interdisciplinary Reviews Water*, *3*(5), 629–657. https://doi.org/10.1002/wat2.1155

Husic, A., Fox, J., Adams, E., Ford, W., Agouridis, C., Currens, J., & Backus, J. (2019). Nitrate pathways, processes, and timing in an agricultural karst system: Development and application of a numerical model. *Water Resources Research*, *55*(3), 2079–2103. https://doi.org/10.1029/2018WR023703

Husic, A., Fox, J., Al Aamery, N., Ford, W., Pollock, E., & Backus, J. (2021). Seasonality of recharge drives spatial and temporal nitrate removal in a karst conduit as evidenced by nitrogen isotope modeling. Journal of geophysical research. *Biogeosciences*, *126*(10), 6454. https://doi.org/10.1029/2021JG006454

Ju, X.-T., Xing, G.-X., Chen, X.-P., Zhang, S.-L., Zhang, L.-J., Liu, X.-J., Cui, Z.-L., Yin, B., Christie, P., Zhu, Z.-L., & Zhang, F. S. (2009). Reducing environmental risk by improving N management in intensive Chinese agricultural systems. *Proceedings of the National Academy of Sciences*, *106*(9), 3041–3046. https://doi.org/10.1073/pnas.0813417106

Kirchner, J. W., Feng, X., & Neal, C. (2000). Fractal stream chemistry and its implications for contaminant transport in catchments. *Nature*, *403*(6769), 524–527. https://doi.org/10.1038/35000537

Knapp, J. L. A., Li, L., & Musolff, A. (2022). Hydrologic connectivity and source heterogeneity control concentration–discharge relationships. *Hydrological Processes*, *36*, e14683.

Knapp, J. L. A., von Freyberg, J., Studer, B., Kiewiet, L., & Kirchner, J. W. (2020). Concentration–discharge relationships vary among hydrological events, reflecting differences in event characteristics. *Hydrology and Earth System Sciences*, *24*(5), 2561–2576. https://doi.org/10.5194/hess-24-2561-2020

Le Mesnil, M., Charlier, J.-B., Moussa, R., & Caballero, Y. (2022). Investigating flood processes in karst catchments by combining concentration-discharge relationship analysis and lateral flow simulation. *Journal of Hydrology*, *605*, 127358. https://doi.org/10.1016/j.jhydrol.2021.127358

Li, J.-Y., & Li, T.-Y. (2018). Seasonal and annual changes in soil/cave air pCO_2 and the δ13CDIC of cave drip water in response to changes in temperature and rainfall. *Applied Geochemistry*, *93*, 94–101. https://doi.org/10.1016/j.apgeochem.2018.04.002

Li, L., Sullivan, P. L., Benettin, P., Cirpka, O. A., Bishop, K., Brantley, S. L., Knapp, J. L. A., Meerveld, I., Rinaldo, A., Seibert, J., Wen, H., & Kirchner, J. W. (2021). Toward catchment hydro-biogeochemical theories. *WIREs Water*, *8*(1), e1495. https://doi.org/10.1002/wat2.1495

Li, X., Wang, J., Lin, J., Yin, W., Shi, Y. Y., Wang, L., Xiao, H. B., Zhong, Z. M., Jiang, H., & Shi, Z. H. (2022). Hysteresis analysis reveals dissolved carbon concentration-discharge relationships during and between storm events. *Water Research*, *226*, 119220.

Liu, W., Tian, S., Youssef, M. A., Birgand, F. P., & Chescheir, G. M. (2022). Patterns of long-term variations of nitrate concentration - stream discharge relationships for a drained agricultural watershed in midwestern USA. *Journal of Hydrology*, *614*, 128479.

Liu, X. J., Fu, Z. Y., Zhang, W., Xiao, S. S., Chen, H. S., & Wang, K. L. (2023). Soluble carbon loss through multiple runoff components in the shallow subsurface of a karst hillslope: Impact of critical zone structure and land use. *Catena*, *222*, 106868.

Lloyd, C. E. M., Freer, J. E., Johnes, P. J., & Collins, A. L. (2016). Using hysteresis analysis of high-resolution water quality monitoring data, including uncertainty, to infer controls on nutrient and sediment transfer in catchments. *Science of the Total Environment*, *543*, 388–404.

Lorette, G., Sebilo, M., Buquet, D., Lastennet, R., Denis, A., Peyraube, N., Charriere, V., & Studer, J. C. (2022). Tracing sources and fate of nitrate in multilayered karstic hydrogeological catchments using natural stable isotopic composition ($\delta^{15}N\text{-}NO_3^-$ and $\delta^{18}O\text{-}NO_3^-$). Application to the Toulon karst system (Dordogne, France). *Journal of Hydrology*, *610*, 127972.

McDonnell, J. J., & Beven, K. (2014). Debates-the future of hydrological sciences: A (common) path forward? A call to action aimed at understanding velocities, celerities and residence time distributions of the headwater hydrograph. *Water Resources Research*, *50*(6), 5342–5350. https://doi.org/10.1002/2013WR015141

Minaudo, C., Dupas, R., Gascuel-Odoux, C., Fovet, O., Mellander, P.-E., Jordan, P., Shore, M., & Moatar, F. (2017). Nonlinear empirical modeling to estimate phosphorus exports using continuous records of turbidity and discharge. *Water Resources Research*, *53*(9), 7590–7606. https://doi.org/10.1002/2017WR020590

Minaudo, C., Dupas, R., Gascuel-Odoux, C., Roubeix, V., Danis, P.-A., & Moatar, F. (2019). Seasonal and event-based concentration-discharge relationships to identify catchment controls on nutrient export regimes. *Advances in Water Resources*, *131*, 103379. https://doi.org/10.1016/j.advwatres.2019.103379

Moatar, F., Abbott, B. W., Minaudo, C., Curie, F., & Pinay, G. (2017). Elemental properties, hydrology, and biology interact to shape concentration-discharge curves for carbon, nutrients, sediment, and major ions. *Water Resources Research*, *53*(2), 1270–1287. https://doi.org/10.1002/2016WR019635

Musolff, A., Fleckenstein, J. H., Rao, P. S. C., & Jawitz, J. W. (2017). Emergent archetype patterns of coupled hydrologic and biogeochemical responses in catchments. *Geophysical Research Letters*, *44*(9), 4143–4151. https://doi.org/10.1002/2017GL072630

Musolff, A., Schmidt, C., Selle, B., & Fleckenstein, J. H. (2015). Catchment controls on solute export. *Advances in Water Resources*, *86*, 133–146. https://doi.org/10.1016/j.advwatres.2015.09.026

Musolff, A., Zhan, Q., Dupas, R., Minaudo, C., Fleckenstein, J. H., Rode, M., Dehaspe, J., & Rinke, K. (2021). Spatial and temporal variability in concentration-discharge relationships at the event scale. *Water Resources Research*, *57*(10), e2020WR029442. https://doi.org/10.1029/2020WR029442

Pesántez, J., Mosquera, G. M., Crespo, P., Breuer, L., & Windhorst, D. (2018). Effect of land cover and hydro-meteorological controls on soil water DOC concentrations in a high-elevation tropical environment. *Hydrological Processes*, *32*(17), 2624–2635. https://doi.org/10.1002/hyp.13224

Qin, C., Li, S.-L., Waldron, S., Yue, F.-J., Wang, Z.-J., Zhong, J., Ding, H., & Liu, C.-Q. (2020). High-frequency monitoring reveals how hydrochemistry and dissolved carbon respond to rainstorms at a karstic critical zone, Southwestern China. *Science of the Total Environment*, *714*, 136833. https://doi.org/10.1016/j.scitotenv.2020.136833

Remondi, F., Kirchner, J. W., Burlando, P., & Fatichi, S. (2018). Water flux tracking with a distributed hydrological model to quantify controls on the spatiotemporal variability of transit time distributions. *Water Resources Research*, *54*(4), 3081–3099. https://doi.org/10.1002/2017WR021689

Rose, L. A., & Karwan, D. L. (2021). Stormflow concentration–discharge dynamics of suspended sediment and dissolved phosphorus in an agricultural watershed. *Hydrological Processes*, *35*(12), XXX. https://doi.org/10.1002/hyp.14455

Rose, L. A., Karwan, D. L., & Godsey, S. E. (2018). Concentration–discharge relationships describe solute and sediment mobilization, reaction, and transport at event and longer timescales. *Hydrological Processes*, *32*(18), 2829–2844. https://doi.org/10.1002/hyp.13235

Rue, G. P., Rock, N. D., Gabor, R. S., Pitlick, J., Tfaily, M., & McKnight, D. M. (2017). Concentration-discharge relationships during an extreme event: Contrasting behavior of solutes and changes to chemical quality of dissolved organic material in the Boulder Creek watershed during the September. *Water Resources Research*, *53*(7), 5276–5297. https://doi.org/10.1002/2016WR019708

Sorensen, J. P. R., Butcher, A. S., Stuart, M. E., & Townsend, B. R. (2015). Nitrate fluctuations at the water table: Implications for recharge processes and solute transport in the chalk aquifer. *Hydrological Processes*, *29*(15), 3355–3367. https://doi.org/10.1002/hyp.10447

Soulsby, C., Birkel, C., Geris, J., Dick, J., Tunaley, C., & Tetzlaff, D. (2015). Stream water age distributions controlled by storage dynamics and nonlinear hydrologic connectivity: Modeling with high-resolution isotope data. *Water Resources Research*, *51*(9), 7759–7776. https://doi.org/10.1002/2015WR017888

Sprenger, M., Stumpp, C., Weiler, M., Aeschbach, W., Allen, S. T., Benettin, P., Dubbert, M., Hartmann, A., Hrachowitz, M., Kirchner, J. W., McDonnell, J. J., Orlowski, N., Penna, D., Pfahl, S., Rinderer, M., Rodriguez, N., Schmidt, M., & Werner, C. (2019). The demographics of water: A review of water ages in the critical zone. *Reviews of Geophysics*, *57*(3), 800–834. https://doi.org/10.1029/2018RG000633

Stewart, B., Shanley, J. B., Kirchner, J. W., Norris, D., Adler, T., Bristol, C., Harpold, A. A., Perdrial, J. N., Rizzo, D. M., Sterle, G., Underwood, K. L., Wen, H., & Li, L. (2022). Streams as mirrors: Reading subsurface water chemistry from stream chemistry. *Water Resources Research*, *58*(1), 29931. https://doi.org/10.1029/2021WR029931

Tan, C. Q. (2020). *Biogeochemical characteristics of carbon and its response to rainstorms in a karst critical zone* [PhD Dissertation Tianjin University]. Tianjin, China.

Tan, K., Xia, Z., & Huang, G. (2015). The fertilizer application current situation and the countermeasures in Guizhou province. *Tillage and Cultivation*, *4*, 46–47 (in Chinese).

Tittel, J., Büttner, O., Friese, K., Lechtenfeld, O. J., Schuth, S., Tümpling, W., & Musolff, A. (2022). Iron exports from catchments are constrained by redox status and topography. *Global Biogeochemical Cycles*, *36*(1), 7056. https://doi.org/10.1029/2021GB007056

Tunaley, C., Tetzlaff, D., Lessels, J., & Soulsby, C. (2016). Linking high-frequency DOC dynamics to the age of connected water sources. *Water Resources Research*, *52*(7), 5232–5247. https://doi.org/10.1002/2015WR018419

van der Velde, Y., Heidbüchel, I., Lyon, S. W., Nyberg, L., Rodhe, A., Bishop, K., & Troch, P. A. (2015). Consequences of mixing assumptions for time-variable travel time distributions. *Hydrological Processes*, *29*, 3460–3474.

Wang, K. (2008). *Research on the characteristics of the epikarst developing in Puding region, Guizhou province southwestern China* [PhD dissertation, Nanjing University], Nanjing, China.

Wang, S., Yan, Y., Fu, Z., & Chen, H. (2022). Rainfall-runoff characteristics and their threshold behaviors on a karst hillslope in a peak-cluster depression region. *Journal of Hydrology*, *605*, 127370. https://doi.org/10.1016/j.jhydrol.2021.127370

Wang, Z.-J., Li, S.-L., Yue, F.-J., Qin, C.-Q., Buckerfield, S., & Zeng, J. (2020). Rainfall driven nitrate transport in agricultural karst surface river system: Insight from high resolution hydrochemistry and nitrate isotopes. *Agriculture, Ecosystems & Environment*, *291*, 106787. https://doi.org/10.1016/j.agee.2019.106787

Westphal, K., Musolff, A., Graeber, D., & Borchardt, D. (2020). Controls of point and diffuse sources lowered riverine nutrient concentrations asynchronously, thereby warping molar N:P ratios. *Environmental Research Letters*, *15*(10), 104009. https://doi.org/10.1088/1748-9326/ab98b6

Winter, C., Lutz, S. R., Musolff, A., Kumar, R., Weber, M., & Fleckenstein, J. H. (2021). Disentangling the impact of catchment heterogeneity on nitrate export dynamics from event to long-term time scales. *Water Resources Research*, *57*(1), e2020WR027992. https://doi.org/10.1029/2020WR027992

Xia, J., Wang, J., Zhang, L., Wang, X., Yuan, W., Anderson, C. W. N., Chen, C., Peng, T., & Feng, X. (2021). Significant mercury efflux from a karst region in Southwest China - results from mass balance studies in two catchments. *Science of the Total Environment*, *769*, 144892. https://doi.org/10.1016/j.scitotenv.2020.144892

Yang, P., Wang, Y., Wu, X., Chang, L., Ham, B., Song, L., & Groves, C. (2020). Nitrate sources and biogeochemical processes in karst underground rivers impacted by different anthropogenic input characteristics. *Environmental Pollution*, *265*, 114835. https://doi.org/10.1016/j.envpol.2020.114835

Yi, Y., Zhong, J., Bao, H., Mostofa, K. M. G., Xu, S., Xiao, H. Y., & Li, S. L. (2021). The impacts of reservoirs on the sources and transport of riverine organic carbon in the karst area: A multi-tracer study. *Water Research*, *194*, 116933.

Yue, F.-J., Li, S.-L., Waldron, S., Wang, Z.-J., Oliver, D. M., Chen, X., & Liu, C.-Q. (2020). Rainfall and conduit drainage combine to accelerate nitrate loss from a karst agroecosystem: Insights from stable isotope tracing and high-frequency nitrate sensing. *Water Research*, *186*, 116388. https://doi.org/10.1016/j.watres.2020.116388

Yue, F.-J., Waldron, S., Li, S.-L., Wang, Z.-J., Zeng, J., Xu, S., Zhang, Z.-C., & Oliver, D. M. (2019). Land use interacts with changes in catchment hydrology to generate chronic nitrate pollution in karst waters and strong seasonality in excess nitrate export. *Science of the Total Environment*, *696*, 134062. https://doi.org/10.1016/j.scitotenv.2019.134062

Zarnetske, J. P., Bouda, M., Abbott, B. W., Saiers, J., & Raymond, P. A. (2018). Generality of hydrologic transport limitation of watershed organic carbon flux across ecoregions of the United States. *Geophysical Research Letters*, *45*(21), 11702–11711. https://doi.org/10.1029/2018GL080005

Zeng, J., Yue, F.-J., Wang, Z.-J., Wu, Q., Qin, C.-Q., & Li, S.-L. (2019). Quantifying depression trapping effect on rainwater chemical composition during the rainy season in karst agricultural area, southwestern China. *Atmospheric Environment*, *218*, 116998. https://doi.org/10.1016/j.atmosenv.2019.116998

Zhang, R., Chen, X., Zhang, Z., & Soulsby, C. (2020). Using hysteretic behaviour and hydrograph classification to identify hydrological function across the "hillslope–depression–stream" continuum in a karst catchment. *Hydrological Processes*, *34*(16), 3464–3480. https://doi.org/10.1002/hyp.13793

Zhang, Y., & Shao, Q. (2018). Uncertainty and its propagation estimation for an integrated water system model: An experiment from water quantity to quality simulations. *Journal of Hydrology*, *565*, 623–635. https://doi.org/10.1016/j.jhydrol.2018.08.070

Zhang, Z., Chen, X., Cheng, Q., Li, S., Yue, F., Peng, T., Waldron, S., Oliver, D. M., & Soulsby, C. (2020). Coupled hydrological and biogeochemical modelling of nitrogen transport in the karst critical zone. *Science of the Total Environment*, *732*, 138902. https://doi.org/10.1016/j.scitotenv.2020.138902

Zhang, Z., Chen, X., Cheng, Q., & Soulsby, C. (2019). Storage dynamics, hydrological connectivity and flux ages in a karst catchment: Conceptual modelling using stable isotopes. *Hydrology and Earth System Sciences*, *23*(1), 51–71. https://doi.org/10.5194/hess-23-51-2019

Zhang, Z., Chen, X., Li, S., Yue, F., Cheng, Q., Peng, T., & Soulsby, C. (2021). Linking nitrate dynamics to water age in underground conduit flows in a karst catchment. *Journal of Hydrology*, *596*, 125699. https://doi.org/10.1016/j.jhydrol.2020.125699

Zhang, Z., Chen, X., & Soulsby, C. (2017). Catchment-scale conceptual modelling of water and solute transport in the dual flow system of the karst critical zone. *Hydrological Processes*, *31*(19), 3421–3436. https://doi.org/10.1002/hyp.11268

Zhi, W., & Li, L. (2020). The shallow and deep hypothesis: Subsurface vertical chemical contrasts shape nitrate export patterns from different land uses. *Environmental Science & Technology*, *54*(19), 11915–11928. https://doi.org/10.1021/acs.est.0c01340

Zhi, W., Li, L., Dong, W., Brown, W., Kaye, J., Steefel, C., & Williams, K. H. (2019). Distinct source water chemistry shapes contrasting concentration-discharge patterns. *Water Resources Research*, *55*(5), 4233–4251. https://doi.org/10.1029/2018WR024257

Zhong, J., Li, S., Tao, F., Yue, F., & Liu, C.-Q. (2017). Sensitivity of chemical weathering and dissolved carbon dynamics to hydrological conditions in a typical karst river. *Scientific Reports*, *7*(1), 42944. https://doi.org/10.1038/srep42944

Zhong, J., Li, S.-L., Liu, J., Ding, H., Sun, X., Xu, S., Wang, T., Ellam, R. M., & Liu, C.-Q. (2018). Climate variability controls on CO2 consumption fluxes and carbon dynamics for monsoonal Rivers: Evidence from Xijiang River, Southwest China. *Journal of Geophysical Research – Biogeosciences*, *123*(8), 2553–2567. https://doi.org/10.1029/2018JG004439

SUPPORTING INFORMATION

Additional supporting information can be found online in the Supporting Information section at the end of this article.

How to cite this article: Hao, L., Zhang, Z., Chen, X., Cheng, Q., Li, S., Yue, F., Peng, T., & Zhang, L. (2023). Intra-event concentration–discharge relationships affected by hydrological connectivity in a karst catchment. *Hydrological Processes*, *37*(4), e14880. https://doi.org/10.1002/hyp.14880